



# Optics Letters

## High extinction ratio on-chip pump-rejection filter based on cascaded grating-assisted contra-directional couplers in silicon nitride rib waveguides

XIAOMIN NIE,<sup>1,2,\*</sup> NINA TURK,<sup>1,2</sup> YANG LI,<sup>1,2</sup> ZUYANG LIU,<sup>1,2</sup> AND ROEL BAETS<sup>1,2</sup> 

<sup>1</sup>Photonics Research Group, INTEC, Ghent University-IMEC, Technologiepark 126, B-9052 Ghent, Belgium

<sup>2</sup>Center for Nano- and Biophotonics, Ghent University, Technologiepark 126, B-9052 Ghent, Belgium

\*Corresponding author: Xiaomin.Nie@UGent.be

Received 19 March 2019; revised 8 April 2019; accepted 8 April 2019; posted 9 April 2019 (Doc. ID 362763); published 26 April 2019

We present an on-chip filter that is based on the grating-assisted contra-directional coupler (GACDC) implemented on a silicon nitride rib waveguide platform. This filter enjoys the benefit of an unlimited free spectral range (FSR) on the red side of the stop/passband. Unlike a Bragg reflector, the GACDC filter has the advantage of coupling the rejected light contra-directionally into a bus waveguide, instead of reflecting it back to the input. This property makes it an add/drop filter suitable for pump rejection and allows effective cascading to provide an even higher extinction ratio compared to the single-stage version. In this Letter, we experimentally demonstrate that a 16-stage cascaded GACDC filter can provide a stop band with a bandwidth smaller than 3 nm and an extinction ratio as high as 68.5 dB. © 2019 Optical Society of America

<https://doi.org/10.1364/OL.44.002310>

Recently, silicon nitride (SiN) has become a highly prominent platform for miniaturizing photonic circuits in the visible or near-infrared range ( $<1 \mu\text{m}$ ), where silicon is not transparent [1]. Like the silicon-on-insulator technology, SiN nanophotonics is also a CMOS-compatible technology that allows for large-scale, cost-effective fabrication of photonic integrated circuits.

A wide range of high-performance components, including grating couplers, polarization splitters, and wavelength selective filters, have been developed on the SiN platform, opening the road to further integration of complex on-chip systems [2,3]. As an essential component, the on-chip wavelength filter is attractive to the researchers interested in on-chip lasers, optical sensors [4], and wavelength-division multiplexers [5]. Filters based on Bragg gratings, ring resonators, and cascaded Mach-Zehnder interferometers (MZIs) have been studied and demonstrated to meet the requirement of various applications [4–6]. Compared to the ring-resonator filters, grating-based filters such as Bragg reflectors have an unlimited free spectral range (FSR). This is important for applications such as on-chip Raman spectroscopic systems [7], which require filters with an

extremely high extinction ratio at the pump wavelength and a flat spectral response in the wavelength range where the Raman Stokes signals are generated. Bragg reflectors can fulfill these requirements. However, to prevent the reflected light from going back to the integrated laser, one would also need to integrate an on-chip circulator, which adds extra complexity and cost to the system. A filter based on the grating-assisted contra-directional coupler (GACDC) provides a better solution. As demonstrated in [8–10], while having a Bragg-grating-defined transfer function, a GACDC filter is able to couple the rejected light contra-directionally into a bus waveguide, instead of reflecting it back to the input. This property allows the GACDC filter to achieve pump rejection without the need for a circulator.

It has been reported that an ultra-high rejection ratio can be achieved by cascaded filters based on ring resonators or MZIs with active phase tuning between the stages [11–13]. However, these solutions have a small FSR precluding their usage as pump-rejection filters in applications that require a broad passband. Grating-based filters exhibit a large FSR and, theoretically, have an arbitrarily high extinction ratio with a sufficient grating length. However, most of the practical implementations have a maximum achievable extinction around 40 dB, limited by the fabrication imperfections [6,14,15]. In this Letter, we report a novel design of cascaded GACDC filters and demonstrate that it can surpass the limitation set by the fabrication errors. As we want to make pump-rejection filters for bio-sensing spectroscopic systems operating in the near-infrared region, the GACDC filters are implemented on the SiN platform, with the center wavelength of the stop band set to 785 nm. This would require gratings with a period smaller than what is possible in conventional 193 nm deep-UV lithography. As a result, we use e-beam lithography for prototyping the proposed devices which, in the future, can also be fabricated by deep-UV immersion lithography in a CMOS fab.

The proposed filters are based on the GACDC, consisting of a narrow and a wide rib waveguide (waveguide  $a$  and  $b$ ), and a grating between them. As shown in Fig. 1(a), a single-stage GACDC filter uses grating couplers as I/O ports and has

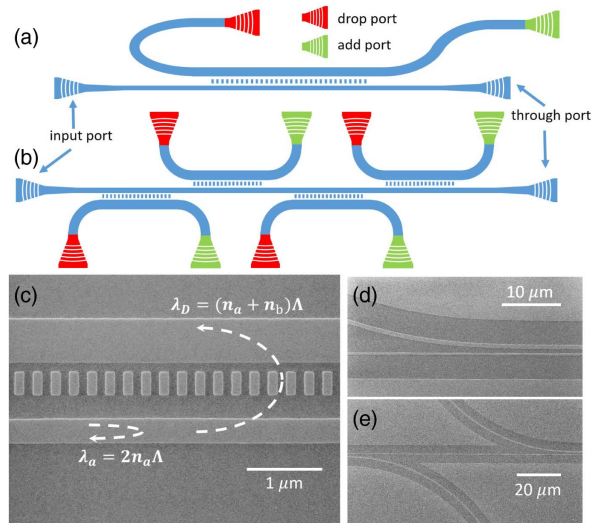


**Fig. 1.** Sketches of (a) the single-stage CDC filter and (b) the four-stage cascaded CDC filter. SEM pictures of (c) the coupler region with illustrations of the intra- and inter-waveguide reflections induced by the contra-directional coupling, (d) the mode-transition region where waveguide  $b$  is approaching waveguide  $a$ , and (e) the mode-transition region in the cascaded GACDC filter.

waveguide tapers to connect them to the GACDC. By connecting multiple GACDCs, one can easily construct a cascaded GACDC filter such as the four-stage cascaded GACDC filter shown in Fig. 1(b). Measured from the scanning electron microscopy (SEM) image of the coupler region shown in Fig. 1(c), the two waveguides have different widths ( $W_a = 330$  nm and  $W_b = 585$  nm). The grating has a width  $W_g = 320$  nm, a period  $\Lambda = 244$  nm, and a duty cycle around 50%. To obtain a proper coupling strength  $\kappa$  (calculated by Eq. (3) in [10]), we separate the two waveguides for 750 nm and laterally shift the grating for 80 nm from the center to waveguide  $b$ . In the mode-transition regions on the two sides of each coupler, we designed bending tapers to bring the two waveguides close and to separate them, as shown in Fig. 1(d), where waveguide  $b$  is approaching waveguide  $a$  and, in Fig. 1(e), which pictures the mode-transition regions of the cascaded GACDC filter.

The working principle is also illustrated in Fig. 1(c). While the co-directional coupling is suppressed by the phase mismatch between the fundamental TE-like modes in waveguides  $a$  and  $b$  (with effective refractive indices  $n_a$  and  $n_b$ ), the contra-directional coupling can be achieved with the assistance of the grating. Injected from the input port, light with wavelength  $\lambda_a = 2n_a\Lambda$  can be reflected back to the input due to the intra-waveguide Bragg reflection, while the inter-waveguide contra-directional coupling can reflect the light with wavelength  $\lambda_D = (n_a + n_b)\Lambda$  to the drop port [16]. As a result, the transmission spectrum measured at the through port will possess two stop bands corresponding to the intra-waveguide Bragg reflection and the inter-waveguide reflection induced by the contra-directional coupling. For the convenience of the discussion, we refer to the two stop bands as the self-reflection band and cross-reflection band. In applications such as on-chip Raman spectroscopy, the latter is used to reject the

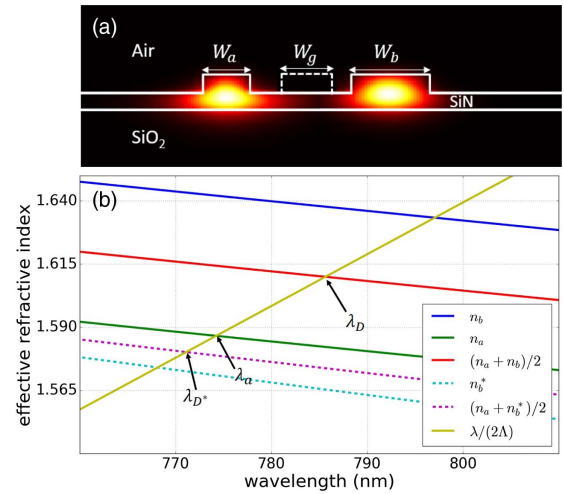


**Fig. 2.** (a) Cross section of the coupler region with the intensity profiles of the fundamental TE-like modes of both rib waveguides; (b) the dispersion curves of the modes with phase-matching wavelengths indicated with arrows and labels.

pump, since there is an unlimited FSR on its red side, and the former (as a side effect of the design) is not used.

We solve the waveguide modes in the coupler region with the mode solver FIMMWARE. Figure 2(a) shows the cross section with the calculated intensity profiles of the fundamental TE-like modes in both rib waveguides. In the simulation, we set both the rib height and slab thickness to 150 nm, and take 1.89 as the material refractive index of SiN [17]. In Fig. 2(b), the effective indices of the modes in both waveguides are plotted as a function of the wavelength. In designing, the waveguide widths are first determined to ensure a large phase mismatch between the fundamental TE-like mode in waveguide  $a$  and the guided modes in waveguide  $b$  to suppress the co-directional coupling. After that, we add the curves of the average indices and  $y = \lambda/(2\Lambda)$  to calculate the grating period that allows matching  $\lambda_D$  to the required reflecting wavelength. In this Letter, we set  $\lambda_D$  to 785 nm and  $\lambda_a$  to 774 nm.

Apart from the position of the stop bands, we are also interested in the achievable extinction ratio. According to mode coupling theory [16], for a grating-based reflector with a total grating length  $L$ , the peak reflection at the center wavelength of the stop band can be written as

$$R = \tanh^2(\kappa L). \quad (1)$$

Theoretically, this means that an arbitrary extinction ratio can be obtained by increasing the total length of the grating. Realistically, however, the extinction ratio typically saturates around 40 dB beyond a certain filter length [6,14,15]. While it has been reported that the extinction ratio can be reduced by the light propagating in the cladding or substrate, as well as the light with a different polarization [11,13], the experiments indicate that, in this Letter, the major mechanism limiting the extinction ratio is the forward scattering caused by the phase errors induced from fabrication imperfections. To understand this, we first think of a Bragg reflector without any fabrication imperfection. In this ideal reflector, the injected light propagating in the forward direction is continuously reflected by the grating units into the backward-propagating

mode. At the Bragg wavelength, the periodicity of the grating units ensures that all partial reflections are in phase and interfere constructively. Although the reflected light propagating in the backward direction needs to travel through the grating and, therefore, is subject to secondary grating diffraction, the resulting contributions to the forward-propagating light will actually be out of phase with the original light coming from the input, thereby helping the input light to decay exponentially. However, in real life, even a very small fabrication imperfection can cause a phase error and create deviations in the phase relationships of all contributing field components. Such a phase error, therefore, will scatter the reflected light and allow a tiny amount of light to travel towards the through port. In addition, as the length of the grating increases, more and more contributions (with phase errors) will play a role and accumulate to set a certain saturation level, limiting the achievable extinction ratio. To surpass this limitation and achieve a higher extinction ratio, an effective way is to remove the reflected light before it can propagate through many grating units [18]. This strategy can be implemented with the cascaded GACDC filters, where the light coupled contra-directionally to the bus waveguides can be coupled out through the drop ports before it can travel too far.

To characterize the fabricated devices, we use a setup containing two cleaved single-mode fibers (780HP) that are positioned near-vertically (10 deg away from normal) to the chip. Light is coupled into and out of the chip through the on-chip grating couplers. A Ti:sapphire tunable CW laser (SOLSTIS, M2) is used to scan over the interested wavelength range with a resolution of 0.3 nm. An optical power meter (HP 8153A) is used to measure the transmitted power.

We first measured the transmission spectra for the single-stage GACDC filters with different filter lengths,  $L = 150, 300, 600, 1000, 2000,$  and  $3000 \mu\text{m}$ . As shown in Fig. 3(a), two notches centered on 772.0 and 783.6 nm are observed corresponding to the self- and cross-reflection bands. A third dip centered at 769.2 nm could be explained by the contra-directional coupling between the forward-propagating mode (with effective refractive index  $n_a$ ) in waveguide  $a$  and a high-order TM-like backward-propagating mode (with effective refractive index  $n_b^*$ ) in waveguide  $b$ . These three wavelengths are in agreement with  $\lambda_a, \lambda_D,$  and  $\lambda_{D^*}$  in Fig. 1(e), with the small discrepancy induced by the uncertainties in the etch depth. Given the input power of around 3 dBm, the average insertion loss is estimated to be 18.8 dB due to the loss of fiber-to-chip coupling.

To better observe the trend of saturation, we need to estimate the average extinction ratio, as the spectral response inside the stop bands is not smooth, especially for the devices with a large filter length. We average the transmitted power measured around the center wavelengths of the stop bands and normalize it to the averaged transmitted power measured outside the stop bands. In Fig. 2(b), we plot the average extinction ratio of both stop bands as a function of the filter length  $L$ , with the error bars indicating the maximum and minimum extinction ratio inside the stop bands. From the curves, we can see that while the average extinction ratio of the cross-reflection band is lower than that of the self-reflection band, they both increase with the filter length. As expected, the increment decreases for a large filter length, and the extinction ratio almost stops increasing and saturates to around 40 dB for  $L$  larger than 2000  $\mu\text{m}$ .

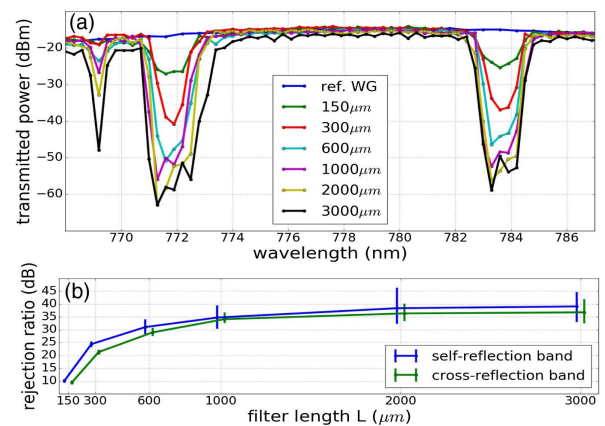


**Fig. 3.** (a) Measured transmission spectra of a reference rib waveguide and GACDC filters with  $L = 150, 300, 600, 1000, 2000,$  and  $3000 \mu\text{m}$ ; (b) the calculated average extinction ratio in both stop bands plotted as a function of the filter length  $L$ . In (b), the two curves are shifted horizontally  $\pm 20 \mu\text{m}$  for better visualization.

Then we measured the transmission spectrum of a set of cascaded GACDC filters that have the same total filter length (2000  $\mu\text{m}$ ) but a different number of stages (4, 8, 10, and 16). The spectra are shown in Fig. 4(a), together with the spectrum measured from a single-stage version and a reference rib waveguide. Figure 4(b) shows the average extinction ratio as a function of the number of stages.

In the cross-reflection band, we can see that the cascaded GACDC filters provide a considerably higher extinction ratio compared to the single-stage version. This is because, while the phase errors introduced by the fabrication imperfections are still there, most of the reflections are coupled out from the drop ports before they can interact with the grating units in previous stages. As the number of stages increases, the reflections are removed more frequently, allowing the filter to suffer less from the phase errors and, therefore, have a higher extinction ratio. Nevertheless, while we remove most of the reflections, a small

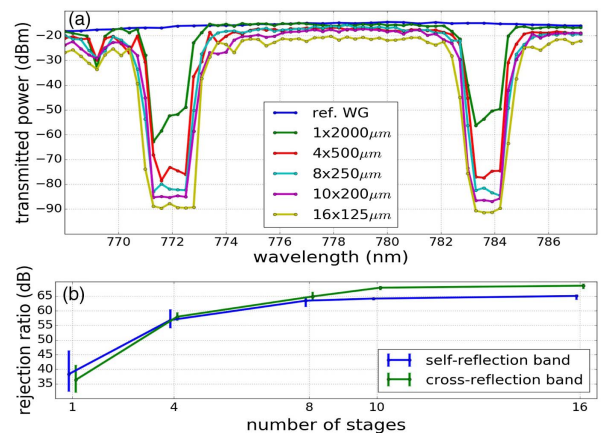


**Fig. 4.** (a) Measured transmission spectra of a reference rib waveguide, a single-stage GACDC filter with  $L = 2000 \mu\text{m}$ , and cascade GACDC filters with the same total length, but a different number of stages (4, 8, 10, and 16); (b) the calculated average extinction ratio in both stop bands plotted as a function of the number of stages. In (b), the two curves are shifted horizontally  $\pm 0.1$  for better visualization.

portion can still survive and be coupled back into waveguide  $a$ . This small portion of reflections, propagating in waveguide  $a$ , is subject to the secondary grating diffraction and, therefore, contributes to the forward-propagating light that can reach the through port, setting a new limitation to the achievable extinction ratio. The spectra shown in Fig. 4(a) and the trend plotted in Fig. 4(b) agree with our expectations. From the 16-stage cascaded GACDC filter, we measured the highest average extinction ratio of up to 68.5 dB in the cross-reflection band with a bandwidth less than 3 nm. The improvement of the achievable extinction ratio is around  $\sim 30$  dB.

Another interesting phenomenon is that the extinction ratio of the self-reflection band is also increased. Nevertheless, it is worth noticing that while the extinction ratio of the cross-reflection band is lower than that of the self-reflection band in the case of a single-stage GACDC filter, now the situation is reversed. This means the extinction ratio in the self-reflection band is improved less than that in the cross-reflection band.

Two possible mechanisms can explain this improvement. The first mechanism relates to the co-directional coupling happening in the mode-transition regions where the two waveguides approach or distance from each other. According to the simulation, only 96.6% of the power stays in waveguide  $a$ , while the rest is co-directionally coupled into waveguide  $b$ . This equals a loss of  $-0.15$  dB per taper if light propagates through it. Such a small loss is negligible for the single-stage GACDC filter, as it only has two tapers. However, for a cascaded GACDC filter with many stages, the total loss experienced by the light propagating directly from the input port to the through port becomes non-negligible. For instance, in the 16-stage cascaded GACDC filter, light traveling through all 32 tapers will experience a total loss of around  $-4.8$  dB. This is the major contribution to the passband loss of around  $-5.6$  dB estimated from the measured spectra in 4(a). For light with wavelengths inside the self-reflection band, the situation is even worse. As an example, in the worst case, light reflected at almost the end of the grating will propagate backward in waveguide  $a$  to almost the beginning of the grating, where it is partly reflected due to a phase error there, reversing its direction and propagating towards the through port. While making it to the through port, this light has to travel through most of the tapers multiple times and, therefore, it is greatly attenuated. More generally, inside the self-reflection band, most of the light has to travel through tapers for multiple times if they want to reach the through port and contribute to the saturation. Consequently, for the cascaded GACDC filters with many stages, the extinction ratio inside the self-reflection band is increased. The second mechanism plays a role in the coupler regions. As the two waveguides are separated only by 750 nm, the fundamental TE-like mode in waveguide  $a$  (with  $W_a = 330$  nm) is loosely confined and slightly pulled to waveguide  $b$ . This means that even though the intra-waveguide reflection happens mostly in waveguide  $a$ , a small amount of light can also be scattered into waveguide  $b$  and can propagate in the backward direction. With this part of light coupled out from the drop ports, we removed the possibility that they could be scattered back again into waveguide  $a$  and propagate to the through port. To some extent, this also helps to increase the extinction ratio inside the self-reflection band.

To summarize, we have demonstrated on-chip GACDC filters that have a cross-reflection band in the near-infrared

wavelength range implemented on a SiN rib waveguide platform. Experimentally, we showed that the average extinction ratio saturates to less than 40 dB for single-stage GACDC filters with a filter length beyond 2000  $\mu\text{m}$ . We also proved a higher extinction ratio can be achieved with the cascaded GACDC filter. For example, a 16-stage cascaded GACDC filter has a cross-reflection band centered at wavelength  $\lambda_D = 783.6$  nm with a bandwidth less than 3 nm and an average extinction ratio up to 68.5 dB. In conclusion, by coupling the rejected light into the bus waveguides, the proposed cascaded GACDC filters can provide a stop band with a very high extinction ratio and an unlimited FSR on the red side of it. These properties make the on-chip GACDC filters suitable and promising for pump rejecting in applications such as on-chip Raman spectroscopy.

**Funding.** Fonds Wetenschappelijk Onderzoek (FWO); China Scholarship Council (CSC); Methusalem; H2020 European Research Council (ERC).

## REFERENCES

1. A. Rahim, E. Ryckeboer, A. Z. Subramanian, S. Clemmen, B. Kuyken, A. Dhakal, A. Raza, A. Hermans, M. Muneeb, S. Dhoore, Y. Li, U. Dave, P. Bienstman, N. Le Thomas, G. Roelkens, D. Van Thourhout, P. Helin, S. Severi, X. Rottenberg, and R. Baets, *J. Lightwave Technol.* **35**, 639 (2017).
2. Y. Zuta, I. Goykhman, B. Desiatov, and U. Levy, *Opt. Express* **18**, 24762 (2010).
3. S. Ramelow, A. Farsi, S. Clemmen, D. Orquiza, K. Luke, M. Lipson, and A. L. Gaeta, "Silicon-nitride platform for narrowband entangled photon generation," arXiv:1508.04358 (2015).
4. K. De Vos, I. Bartolozzi, E. Schacht, P. Bienstman, and R. Baets, *Opt. Express* **15**, 7610 (2007).
5. F. Horst, W. M. Green, S. Assefa, S. M. Shank, Y. A. Vlasov, and B. J. Offrein, *Opt. Express* **21**, 11652 (2013).
6. X. Wang, W. Shi, R. Vafaei, N. A. Jaeger, and L. Chrostowski, *IEEE Photonics Technol. Lett.* **23**, 290 (2011).
7. A. Dhakal, A. Z. Subramanian, P. Wuytens, F. Peyskens, N. Le Thomas, and R. Baets, *Opt. Lett.* **39**, 4025 (2014).
8. M. Qiu, M. Mulot, M. Swillo, S. Anand, B. Jaskorzynska, A. Karlsson, M. Kamp, and A. Forchel, *Appl. Phys. Lett.* **83**, 5121 (2003).
9. D. Tan, K. Ikeda, and Y. Fainman, *Appl. Phys. Lett.* **95**, 141109 (2009).
10. W. Shi, X. Wang, W. Zhang, L. Chrostowski, and N. Jaeger, *Opt. Lett.* **36**, 3999 (2011).
11. N. C. Harris, D. Grassani, A. Simbula, M. Pant, M. Galli, T. Baehr-Jones, M. Hochberg, D. Englund, D. Bajoni, and C. Galland, *Phys. Rev. X* **4**, 041047 (2014).
12. J. R. Ong, R. Kumar, and S. Mookherjee, *IEEE Photonics Technol. Lett.* **25**, 1543 (2013).
13. M. Piekarek, D. Bonneau, S. Miki, T. Yamashita, M. Fujiwara, M. Sasaki, H. Terai, M. G. Tanner, C. M. Natarajan, R. H. Hadfield, and J. L. O'Brien, *Opt. Lett.* **42**, 815 (2017).
14. J. Wang, I. Glesk, and L. Chen, *Electron. Lett.* **51**, 712 (2015).
15. D. Pérez-Galacho, C. Alonso-Ramos, F. Mazeas, X. Le Roux, D. Oser, W. Zhang, D. Marris-Morini, L. Labonté, S. Tanzilli, E. Cassan, and L. Vivien, *Opt. Lett.* **42**, 1468 (2017).
16. P. Yeh and H. Taylor, *Appl. Opt.* **19**, 2848 (1980).
17. A. Subramanian, P. Neutens, A. Dhakal, R. Jansen, T. Claes, X. Rottenberg, F. Peyskens, S. Selvaraja, P. Helin, B. Du Bois, and K. Leyssens, *IEEE Photonics J.* **5**, 2202809 (2013).
18. D. Oser, F. Mazeas, X. L. Roux, D. Pérez-Galacho, O. Alibart, S. Tanzilli, L. Labonté, D. Marris-Morini, L. Vivien, E. Cassan, and C. Alonso-Ramos, "Coherency-broken Bragg filters: surpassing on-chip rejection limitations," arXiv:1806.08833 (2018).